Structure factors and x-ray diffraction intensities in molten alkali halides

Journal of Physics Communications

PAPER

Structure factors and x-ray diffraction intensities in molten alkali halides

Maria C Abramo[1], **Dino Costa**[1], **Gianpietro Malescio**[1], **Gianmarco Munaò**[1], **Giuseppe Pellicane**[2,3], **Santi Prestipino**[1] **and Carlo Caccamo**[1]

[1] Dipartimento di Scienze Matematiche e Informatiche, Scienze Fisiche e Scienze della Terra, Università degli Studi di Messina, Viale F. Stagno d'Alcontres 31—98166 Messina, Italy
[2] Dipartimento di Scienze Biomediche, Odontoiatriche e delle Immagini Morfologiche e Funzionali, Università degli Studi di Messina, Via Consolare Valeria 1 (Azienda Ospedaliera Universitaria Policlinico 'G. Martino')—98125 Messina, Italy
[3] School of Chemistry and Physics, University of Kwazulu-Natal, Private Bag X01, Scottsville 3209—Pietermaritzburg, South Africa

E-mail: carlo.caccamo@unime.it

Keywords: molten salts, computer simulation, x-ray diffraction

OPEN ACCESS

RECEIVED
2 June 2020

REVISED
20 June 2020

ACCEPTED FOR PUBLICATION
3 July 2020

PUBLISHED
21 July 2020

Abstract

We show by extensive molecular dynamics simulations that rather accurate predictions of structure factors and x-ray diffraction intensities of molten alkali halides can be achieved in terms of the Born-Huggins-Mayer-Fumi-Tosi rigid ion potential description of these systems. Specifically, the partial structure factors of six ionic melts, namely NaCl, RbCl, LiCl, LiF, NaF and KF, are computed by Fourier inversion of the radial distribution functions obtained from simulation; the x-ray diffraction intensity is then obtained from the calculated partial structure factors. We perform a comparison between the molecular dynamics results and the experimental data obtained via neutron and/or x-ray diffraction. We also determine the total number density and total charge structure factors and document that, in all the salts examined, the peaks in the x-ray intensities fall at wavevectors practically coincident with those of the partial and total structure factors. We then show how to improve upon some limits emerging in the adopted model when applied to molten fluorides. We finally comment on the opportunity to extend to other molten alkali halides, for which experimental x-ray diffraction intensities are available, the assessment of structural predictions according to the scheme outlined here.

1. Introduction

Molten salts and their mixtures are of current interest both for fundamental statistical-mechanical motivations, and for a number of technological applications mostly in the energy production and storage fields [1–6]. Recently we have undertaken a molecular dynamics (MD) investigation of thermodynamic quantities and liquid-vapor coexistence conditions in molten alkali-halides [7]. This study was performed by employing the well known Born-Huggins-Mayer-Fumi-Tosi (BHMFT) [8] rigid ion potential to describe particle interactions.

Unlike phase diagrams, the structural properties of molten alkali halides have been intensively investigated over the 1970s and 1980s in simulations employing the BHMFT potential [9–17]. Recent applications of this same interaction law to molten alkali halide mixtures have also been reported [18–21]. Other model potentials have also been the subject of simulation studies in the past (see e.g. [22] and references therein). In all these studies, however, calculations were focussed on the determination of the radial distribution functions of the systems at issue. When possible, these functions were compared to their 'experimental' counterparts as obtained via Fourier transform of the partial structure factors obtained experimentally from neutron diffraction [23–28] or via other methods [29, 30]. Total radial distribution functions have also been computed from x-ray diffraction intensities $I(k)$ (k being the wavevector modulus) [31–34]. The accuracy of the procedures employed in generating real space information from reciprocal space functions, is somehow limited by the fact that the wavevector range covered in the experiments (either neutron or x-ray) is truncated both in the low and in the

high k region, which obviously affects the reliability of the Fourier inversion [14, 15]. Moreover, there are relatively few salts for which the partial structure factors can be determined from neutron diffraction experiments via the isotopic substitution technique [23–28] or otherwise [29].

While, as just cited, there are plenty of simulation investigations of radial distribution functions, similar computations of partial structure factors, $S_{ij}(k)$, are quite scarce. Actually, we are aware of only a few such calculations published long time ago [14–16, 22]. One reason for this relative lack of data is that the estimate, within any simulation strategy, of the $S_{ij}(k)$ requires the use of large boxes, that is of a large number of particles, and long simulation runs in order to gather sufficient statistics [14–16]. These two requirements ask for a considerable computational effort which challenged the resources available decades ago, thereby preventing the assessment of the $S_{ij}(k)$ against the neutron experimental evidence. As for the comparison with x-ray data, the related diffraction intensity $I(k)$ can *indeed* be calculated, as we shall illustrate, from the $S_{ij}(k)$; however, to the best of our knowledge, no such a comparison has hitherto been reported for the $I(k)$ so determined, for either the BHMFT or other model potentials. In this respect, we can only quote a study published long time ago, co-authored by two of us [35], wherein theoretical $S_{ij}(k)$ and $I(k)$ were reported for all alkali-halide melts. In that case the ionic liquids were modeled as charged hard-sphere fluids but no simulations were performed, and the $S_{ij}(k)$ were obtained by means of an integral equation theory.

In this paper we address a systematic investigation through computer simulation of the $S_{ij}(k)$ of several molten alkali halides, specifically NaCl, RbCl, LiCl, LiF, NaF and KF. Calculations will be performed using the BHMFT potential to describe particle interactions, and the $S_{ij}(k)$ of each system will be determined by Fourier transform of the MD radial distribution functions; in order to grant sufficient accuracy of the latter functions, we employ a large number of particles and long simulation runs. Then, the $I(k)$ will be computed as a simple combination of the $S_{ij}(k)$ weighted through the x-ray atomic form factors.

The $S_{ij}(k)$ and $I(k)$ so determined will be first compared to the corresponding experimental quantities for some molten alkali halides for which neutron [23, 25, 27, 28] and x-ray diffraction [31–34] experiments have been performed. Our study will then be extended to molten alkali halides for which only experimental $I(k)$, but no $S_{ij}(k)$, are present.

The paper is organized as follows: the model potential and the simulation techniques are described in section 2. Section 3 contains MD calculations of the partial structure factors and of the x-ray diffraction intensities of the molten alkali halides investigated, together with the comparison with the related neutron and x-ray diffraction data. A discussion of the utility of the present study in the more general scenario of applications of model potentials to describe molten alkali halides is also given. The conclusions follow in section 4.

2. Model and simulation techniques

We recall here the BHMFT potential description of molten alkali halides by referring the reader to [7] for more details.

The interionic potential is written as:

$$v_{ij}(r) = \frac{Z_i Z_j e^2}{r} + A\gamma_{ij} \mathrm{e}^{(\sigma_i+\sigma_j-r)\alpha} - \frac{C_{ij}}{r^6} - \frac{D_{ij}}{r^8}, \tag{1}$$

σ_i being the radius of the i-th ionic species as determined by Fumi and Tosi (FT) [8]. In (1) $Z_i = \pm 1$ is the ionic charge, $A = 0.338 \times 10^{-17}$ joule (equal for all alkali halides), $\gamma_{ij} = 1 + Z_i/n_i + Z_j/n_j$ with $n_i, n_j = 8$ except for $n_{\mathrm{Li}^+} = 2$, α is a parameter which varies from salt to salt, C_{ij} and D_{ij} are van der Waals coefficients [8, 14].

We perform extensive molecular dynamics (MD) simulations under constant number of particles, volume and temperature conditions (NVT ensemble), by always employing no less than $N = 1024$ molecules (i.e. 2048 ions) and up to 4092 molecules (8192 ions) with a box edge ranging from 40 to 75 Å. This allows us to estimate the radial distribution functions, $g_{ij}(r)$ (r being the interparticle distance and (i, j) labels of ionic species), up to rather large r values. High statistical accuracy and smoothness of the $g_{ij}(r)$ have been obtained by generating a very large number of configurations; every simulation run has lasted no less than 200.000 steps, 50 000 to 100 000 of which have been used for the equilibration of the system, with a time step $5 \times 10^{-15} s$, thus covering a total simulation time not shorter than 1 ns. We have checked that such a truncation of the run anyhow ensures the condition that averages over sub-blocks of the total production run yield stable results.

The $S_{ij}(k)$ are obtained by Fourier transforming the $g_{ij}(r)$ according to the definition:

$$S_{ij}(k) = \delta_{ij} + 4\pi\sqrt{\rho_i \rho_j} \int_0^\infty [g_{ij}(r) - 1] \frac{\sin(kr)}{kr} r^2 \mathrm{d}r, \tag{2}$$

where ρ_i is the number density of particles of the i-th ionic species. In this manner we obtain estimates of the $S_{ij}(k)$ which turn out to be rather accurate down to significantly low wavevectors, in some cases even smaller than 0.5 Å^{-1}. In order to assess the $S_{ij}(k)$ obtained via Fourier transform, the same functions have also been

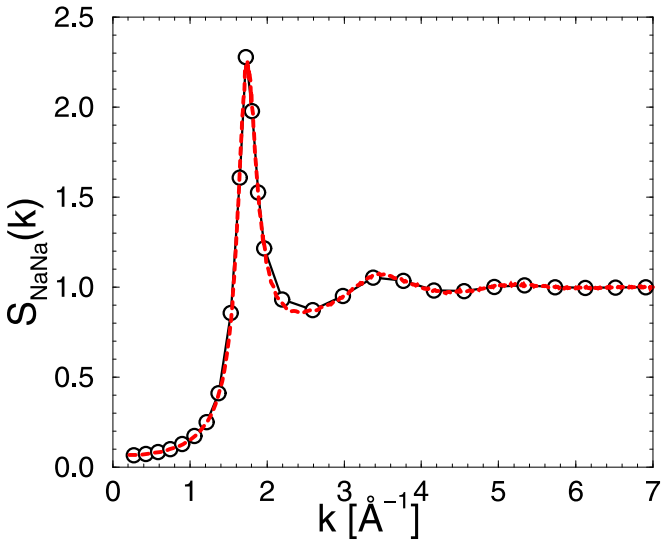

Figure 1. $S_{NaNa}(k)$ at $T = 1148$ K, as obtained through MD via Fourier transform of $g_{NaNa}(r)$ (black line with open circles) and from the density-density correlation function $\langle \rho_{\mathbf{k}} \rho_{-\mathbf{k}} \rangle$ (red dashed line) (see text).

determined, in selected cases, via an estimate of the k-space density-density correlation function $\langle \rho_{\mathbf{k}} \rho_{-\mathbf{k}} \rangle$, where $\rho_{\mathbf{k}}$ is the Fourier transform of the number density function and the average $\langle \cdots \rangle$ is taken over the equilibrium portion of the simulation run [36]. We find that the $S_{ij}(k)$ so obtained fully reproduce those computed via Fourier transform of the $g_{ij}(r)$ within 1% accuracy and down to less than 0.5Å^{-1}. This is shown in figure 1, where we take as an example the case of $S_{NaNa}(k)$ of NaCl at $T = 1148$ K (which is also displayed in comparison to neutron scattering data in figure 3).

We have also verified that at wavevector as small as 0.2–0.3 Å^{-1} the MD $S_{ij}(k)$ tend to reproduce, to within 5%–10% accuracy, the exact $k = 0$ limit [35, 37]

$$S_{ij}(0) = \rho_{\mathrm{M}} k_{\mathrm{B}} T \kappa_{\mathrm{T}}, \tag{3}$$

where ρ_{M} is the molecular number density of particles, k_{B} is the Boltzmann constant, T is the temperature and κ_{T} is the isothermal compressibility. Obviously, the approximations inherent to the BHMFT model also affect such a comparison (see [7] for the accuracy of the isothermal compressibility predictions of the BHMFT potential).

In the next section we shall thoroughly show a comparison between MD computations and neutron diffraction measurements of partial structure factors. In the experimental literature these are usually termed $a_{ij}(k)$, and are defined as follows:

$$a_{ij}(k) = 1 + 4\pi\rho \int_0^\infty [g_{ij}(r) - 1] \frac{\sin(kr)}{kr} r^2 \mathrm{d}r, \tag{4}$$

where ρ is the total number density of particles. As can be seen, the $a_{ij}(k)$ are slightly different from the $S_{ij}(k)$, and we determine the former from the MD estimates of the latter through the relationship

$$a_{ij}(k) = 1 + 2[S_{ij}(k) - \delta_{ij}]. \tag{5}$$

In what follows we shall also resort to the inverse formula

$$S_{ij}(k) = \delta_{ij} + \frac{a_{ij}(k) - 1}{2}. \tag{6}$$

As done earlier [35], we shall additionaly make use of structure factors of global variables namely functions expressing correlations between total number density fluctuations defined as [35, 37–39]

$$S_{\mathrm{NN}}(k) = S_{11}(k) + S_{22}(k) + 2S_{12}(k), \tag{7}$$

and between total charge fluctuations defined as

$$S_{\mathrm{QQ}}(k) = S_{11}(k) + S_{22}(k) - 2S_{12}(k). \tag{8}$$

We also recall the definition of the r-space counterpart of $S_{\mathrm{NN}}(k)$, namely the total density-density radial distribution function [37–39],

$$g_{\mathrm{NN}}(r) = \frac{1}{2}[g_{11}(r) + g_{22}(r) + 2g_{12}(r)]. \tag{9}$$

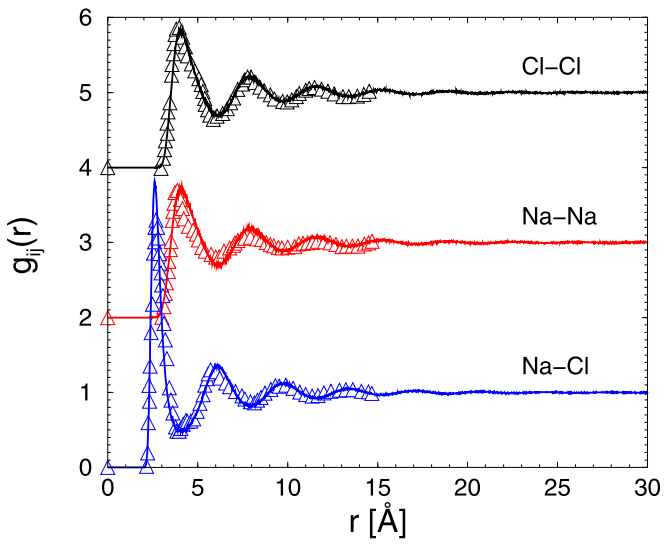

Figure 2. Real-space correlations of NaCl at $T = 1148$ K from MD (lines) and neutrons (symbols) [23]. In order to avoid curves' overlaps, $g_{\mathrm{ClCl}}(r)$ and $g_{\mathrm{NaNa}}(r)$ have been shifted upward by 4 and 2, respectively.

Once the MD $S_{ij}(k)$ have been determined, we calculate the total x-ray diffraction intensity through the formula [35, 40]:

$$I(k) = F_1^2(k)S_{11}(k) + F_2^2(k)S_{22}(k) + 2F_1(k)F_2(k)S_{12}(k) + I_{\mathrm{inc}}(k); \tag{10}$$

here the $F_i(k)$ are the x-ray form factors, which we take from the available tables [41], and $I_{\mathrm{inc}}(k)$ is the incoherent contribution to the scattered intensity [42]. We then reformulate, for future use, equation (10) in terms of $S_{\mathrm{NN}}(k)$ and $S_{\mathrm{QQ}}(k)$, viz.

$$I(k) = C_{\mathrm{NN}}(k) + C_{\mathrm{QQ}}(k) + C_{\mathrm{mix}}(k) + I_{\mathrm{inc}}(k), \tag{11}$$

where

$$C_{\mathrm{NN}}(k) = [F_1(k) + F_2(k)]^2 S_{\mathrm{NN}}(k)/4 \tag{12}$$

$$C_{\mathrm{QQ}}(k) = [F_1(k) - F_2(k)]^2 S_{\mathrm{QQ}}(k)/4 \tag{13}$$

$$C_{\mathrm{mix}}(k) = [F_1^2(k) - F_2^2(k)][S_{11}(k) - S_{22}(k)]/2. \tag{14}$$

3. Results

As anticipated in the Introduction, we first report MD results for some of the molten alkali halides for which neutron diffraction experiments have been performed. In particular, we shall consider NaCl [23], RbCl [25], and LiCl [27, 28]. The MD $a_{ij}(k)$, determined from the $S_{ij}(k)$ through (5), are compared to their experimental counterparts. Then, the x-ray diffraction intensities for the same alkali halides will also be examined. Results for LiF, NaF and KF, for which only x-ray diffraction data are available, will follow next.

As far as radial distribution functions are concerned, these latter have been thoroughly investigated in the past via simulation of the same BHMFT model here used, as anticipated in the Introduction . We shall here report $g_{ij}(r)$ only in two cases (NaCl and NaF) while an extensive analysis of these functions will be the subject of a future paper.

3.1. Chlorides

We first report results for molten NaCl. We show in this case the complete set of structural data we have studied, namely $g_{ij}(r)$, $a_{ij}(k)$, $S_{\mathrm{NN}}(k)$, $S_{\mathrm{QQ}}(k)$, and $I(k)$.

In figure 2 we report the $g_{ij}(r)$ up to 30 Å (actually calculated up to 40 Å) where tail oscillations around 1 appear essentially vanished; moreover, the patterns are quite smooth with negligible statistical noise. The agreement of the MD $g_{ij}(r)$ with those obtained via Fourier inversion from neutron $a_{ij}(k)$ [23], is as good as that reported by other authors [14]. Next, we show in the top panel of figure 3 the $a_{ij}(k)$ obtained from the MD $S_{ij}(k)$ (see(5)) and compare the results with the experimental patterns. It appears that all the main peak positions of the experimental $a_{ij}(k)$ are quantitatively reproduced by the MD patterns. The main peak height in $a_{\mathrm{ClCl}}(k)$ and the

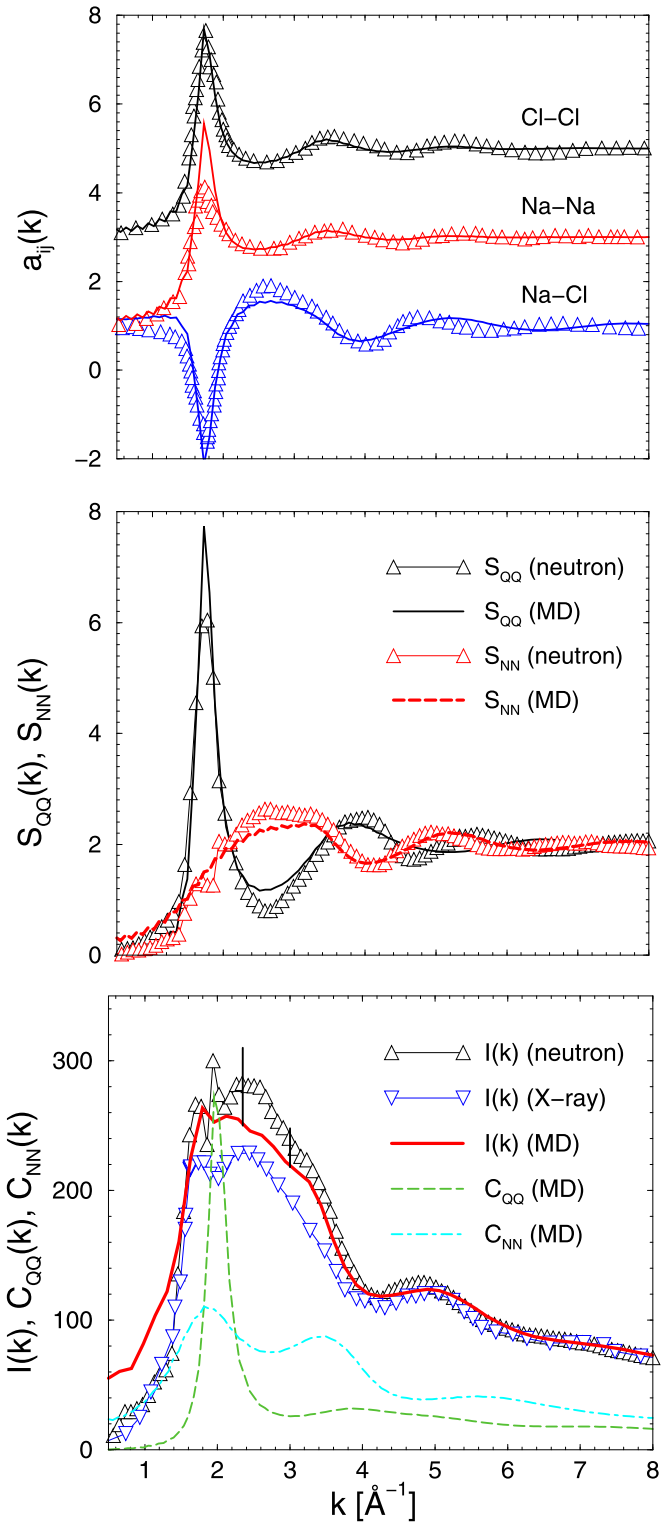

Figure 3. Structural properties of NaCl from MD (lines, $T = 1148$ K), neutrons (triangles up, $T = 1148$ K) [23] and x-rays (triangles down, $T = 1093$ K) [32]. In the top panel, $a_{\mathrm{ClCl}}(k)$ and $a_{\mathrm{NaNa}}(k)$ are shifted upward by 4 and 2 units, respectively. Error bars of $a_{\mathrm{NaNa}}(k)$ have dimensions comparable to the symbols. In the bottom panel, the neutron $I(k)$ is obtained from the neutron $a_{ij}(k)$ through (6) and (10). Error bars on the neutron-derived pattern are also shown. Middle panel: see also note [39].

depth of the first minimum in $a_{\mathrm{NaCl}}(k)$ also appear correctly predicted. An estimate of the $a_{ij}(k)$ for molten NaCl, reported in [14], appears to be in substantial agreement with our data for $k > 1\text{Å}^{-1}$.

The density and charge ordering of the ionic species is described by $S_{\mathrm{NN}}(k)$ and $S_{\mathrm{QQ}}(k)$, which we determine via (7) and (8) from both MD and experimental $S_{ij}(k)$ (the latter being easily derived from the $a_{ij}(k)$ through (6)). These are shown in the central panel of figure 3. The peak in $S_{\mathrm{QQ}}(k)$ obviously falls in correspondence with the first peaks in $\mathrm{S_{NaNa}}(k)$ and $\mathrm{S_{ClCl}}(k)$ and with the first minimum in $\mathrm{S_{NaCl}}(k)$ (see (8)); its height, together with the

pronounced tail oscillations at high k values, signals a well defined charge ordering in this ionic liquid. In comparison, the main features of $S_{NN}(k)$ are significantly less pronounced. Both these two structure factors appear quite well reproduced by MD. Previous estimates of S_{NN} and S_{QQ} [43] are in quite good agreement with those here reported.

In the bottom panel of figure 3, we compare our MD $I(k)$ with the experimental one [32]. The latter exhibits two closely-spaced peaks at relatively low wavectors. The first of these peaks falls at the same k as that of the main peak in the neutron S_{NaNa} and S_{ClCl}, and of the first minimum in S_{NaCl} (see top panel); it also falls in coincidence with the first peak in $S_{QQ}(k)$ (see central panel of the same figure). The second maximum at $k \simeq 2.4$ Å^{-1}, falls near the first peak of the $S_{NN}(k)$ (central panel) placed at $\simeq$2.7 Å^{-1}. The MD $I(k)$ appears to somehow overestimate the heights of these two peaks in the experimental $I(k)$, and such a twofold structure is only visible as a shoulder of the main peak in the MD intensity. Finally, the position of the third maximum in $I(k)$ corresponds quite well with that of the second maximum of $S_{NN}(k)$.

In the bottom panel of figure 3 we also report the functions $C_{NN}(k)$ and $C_{QQ}(k)$ contributing to $I(k)$ in (11). These two functions have their main maximum falling in correspondence with the twin peaks in the x-ray intensity previously discussed, and represent the major contributions to $I(k)$. Note that the relative amplitudes of these two contributions can be dramatically different in going from one salt to another, due to the interplay of the $F_i(k)$ entering their definitions. In particular, $C_{QQ}(k)$ tends to vanish more the closer the ions forming the salt are to an iso-electronic configuration (see below). In figure 3 we also report the $I(k)$ obtained from neutron $a_{ij}(k)$ [23] at 1148K, by using (6) to obtain the experimental $S_{ij}(k)$. The overall pattern is sensibly higher than the one obtained at 1093 K through x-ray diffraction [32]. In our opinion, the different temperature in the two experiments can hardly be deemed as source of such a discrepancy [35]. It seems more likely that the unavoidable uncertainties in the procedure of reconstruction of the partial diffraction patterns through isotopic substitution, which are indeed significant in $a_{NaNa}(k)$ (see [23] and caption of figure 2), are the reason for such a disagreement.

Results for RbCl are reported in figure 4. The MD $a_{ij}(k)$ are compared with the experimental curves in the top panel. Overall, the agreement with the neutron data appears good; a small discrepancy is only visible in the height of the first maximum of $a_{NaCl}(k)$. In the central panel of figure 4 we show the total structure factors. The MD $S_{NN}(k)$ appears accurate against experiment; the high peak in $S_{QQ}(k)$ is also reasonably well reproduced. In comparison, the main features of $S_{NN}(k)$ are substantially less pronounced. Finally, in the bottom panel of figure 4 we show the x-ray diffraction intensity. Here we can only produce a comparison between the MD $I(k)$ and that obtained through (10) by using the neutron $S_{ij}(k)$ calculated, as before, from the experimental $a_{ij}(k)$ via (6). In fact, as far as we know, there are no published x-ray diffraction data for molten RbCl. It appears that the diffraction pattern obtained from simulation correctly reproduces the positions of the main features of the x-ray $I(k)$ as obtained from neutron data; at the same time it overestimates the height of the first peak, which MD predicts only as a shoulder, while the main peak height is underestimated. The second maximum in $I(k)$ at $\simeq$4 Å^{-1} is instead quite well reproduced and, as found in NaCl, it falls in correspondence with the second maximum in $S_{NN}(k)$.

The emerging connection between the main features of charge/density fluctuation correlations and x-ray diffraction maxima was originally pointed out in [35]; we shall see that the same connection is also found in the other salts we are going to examine.

In figure 5 we show results for LiCl. As is visible in the top panel, the agreement of the MD $a_{ij}(k)$ with experiment [27, 28] is again sufficiently accurate as far as the positions of the main features and oscillations are concerned. $I(k)$ is displayed in the bottom panel of figure 5. The agreement of MD with the experimental pattern is satisfactory. It is worth mentioning that in this molten salt the x-ray $I(k)$ is characterized by a unique and relatively sharp peak at $k \simeq 2.5$ Å^{-1}, instead of the double peak structure present in NaCl and RbCl. The reason is that, in this case, the first maxima of $S_{QQ}(k)$ and $S_{NN}(k)$ fall at practically the same wavevector (see central panel of figure 5), and according to (11) this results in a cooperative enhancing effect on $I(k)$. Similarly, as found for the previous two salts, the second maximum of $S_{NN}(k)$ leads to the secondary feature of $I(k)$ at 3.5 Å^{-1}.

3.2. Fluorides

The $I(k)$ of molten LiF is displayed in the bottom panel of figure 6. The agreement between MD and experiment is quite good. In the top panel we report MD $S_{NN}(k)$ and $S_{QQ}(k)$ instead of the $a_{ij}(k)$ for which no neutron data are available to compare with. It is particularly clear how the high $S_{QQ}(k)$ peak and the first (and lower) maximum of $S_{NN}(k)$ combine to give rise to the pronounced peak in $I(k)$ while, as seen before, the second maximum in $S_{NN}(k)$ at 4.5 Å^{-1} gives origin to the second maximum in $I(k)$.

In figure 7 we show results for NaF. It immediately appears that the MD $I(k)$ markedly differs from the experimental one: indeed, the simulation pattern has a double maxima structure totally absent in the experimental diffraction pattern; the latter only exhibits a unique main peak at $\simeq$2.7 Å^{-1}, similarly to what

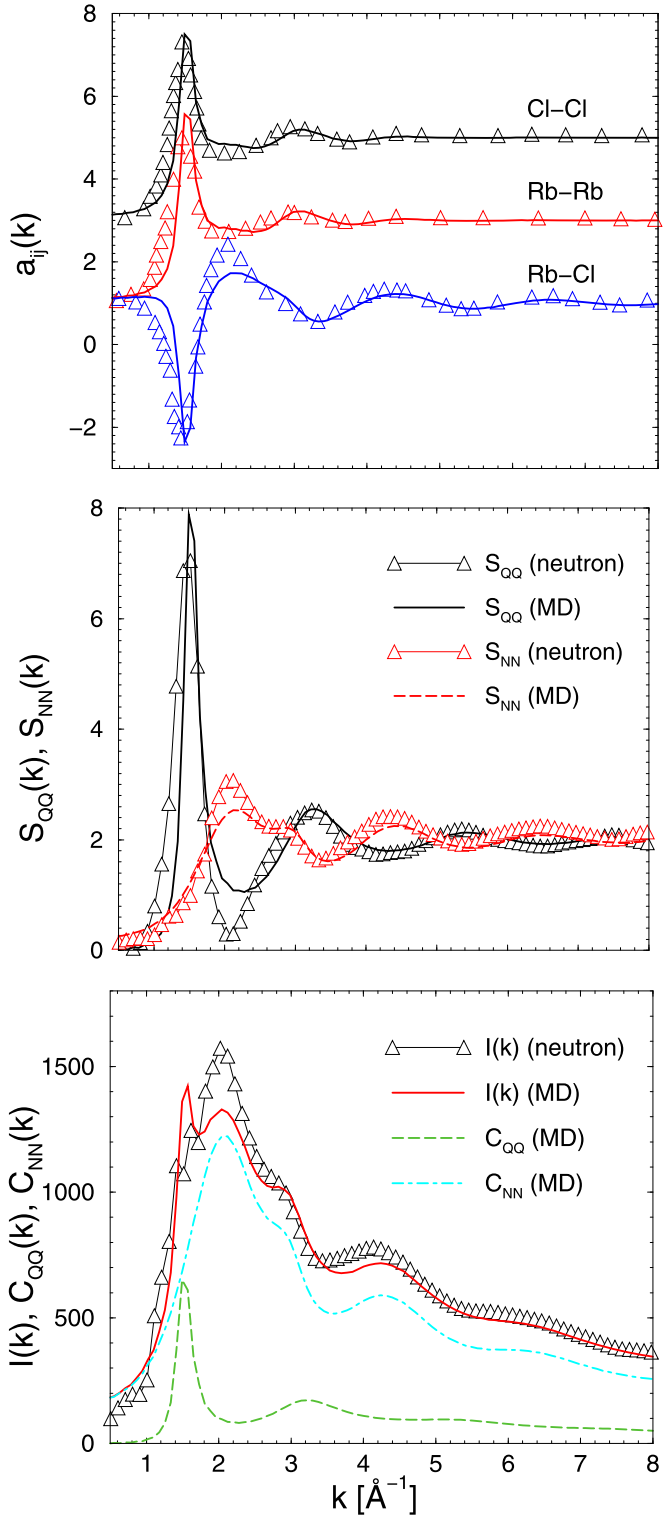

Figure 4. Structural properties of RbCl at $T = 1023$ K from MD (lines) and neutrons (triangles up) [25]. In the top panel, $a_{\mathrm{ClCl}}(k)$ and $a_{\mathrm{RbRb}}(k)$ are shifted upward by 4 and 2 units, respectively. Bottom panel: neutron $I(k)$ obtained as said in the caption of figure 2.

happened for LiCl and LiF, but visibly broader. In this respect, we note that NaF is formed by the iso-electronic Na^+ and F^- ions; for this reason $C_{QQ}(k)$ tends to vanish, so that the main peak of the MD $I(k)$ falls in correspondence with the first maximum of the BHMFT density-density correlation function $S_{NN}(k)$ at $k \simeq 2$ Å^{-1} (see central panel of figure 7).

The inadequacy of the BHMFT prediction in the present fluoride salt case appears at variance of the previously illustrated (relative) successes. In this respect, we recall that some inadequacy of the Huggins-Mayer representation of interactions in alkali fluorides was already signalled in simulations of those systems [12]. We

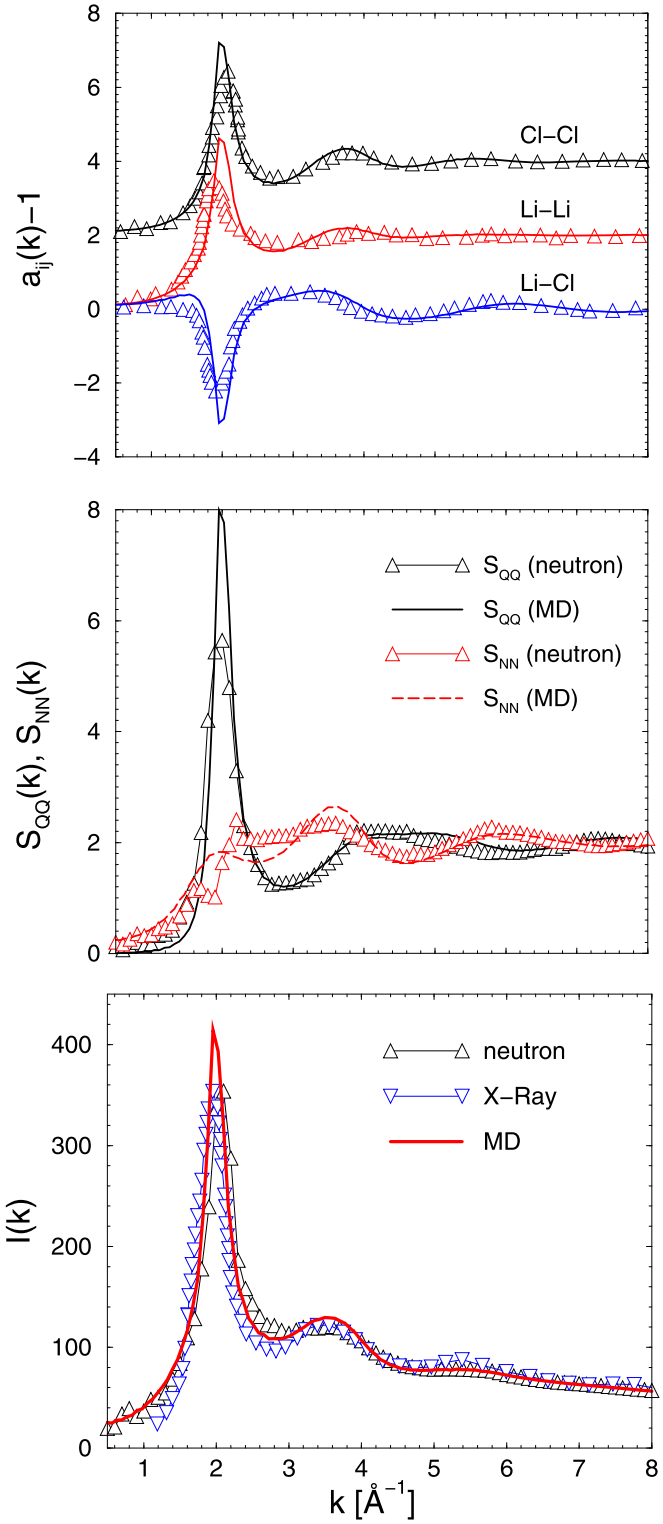

Figure 5. Structural properties of LiCl at $T = 900$ K from MD (lines), neutrons (triangles up) [27, 28] and x-rays (triangles down) [32]. In the top panel, $a_{\mathrm{ClCl}}(k)$ and $a_{\mathrm{LiLi}}(k)$ are shifted upward by 4 and 2 units, respectively. Bottom panel: neutron $I(k)$ obtained as said in the caption of figure 2.

also note that the less sophisticated charged hard sphere model adopted in [35] yielded a better agreement with the experimental $I(k)$ than here just shown. This prompts us to revisit the BHMFT description of repulsive effects at short range for the *molten* NaF case. To this aim we adopt in (1) an exponent higher than the FT $\alpha = 3.03$. After several trials, we choose the value $\alpha = 5$ which yields the best fit overall to the experimental $I(k)$. The result is shown in the central and bottom panels of figure 7. We see that the MD $I(k)$ now exhibits a *unique* main maximum whose position is in quite good agreement with experiment though its height is sensibly overestimated. The same can be said for the positions and heights of the secondary features of $I(k)$.

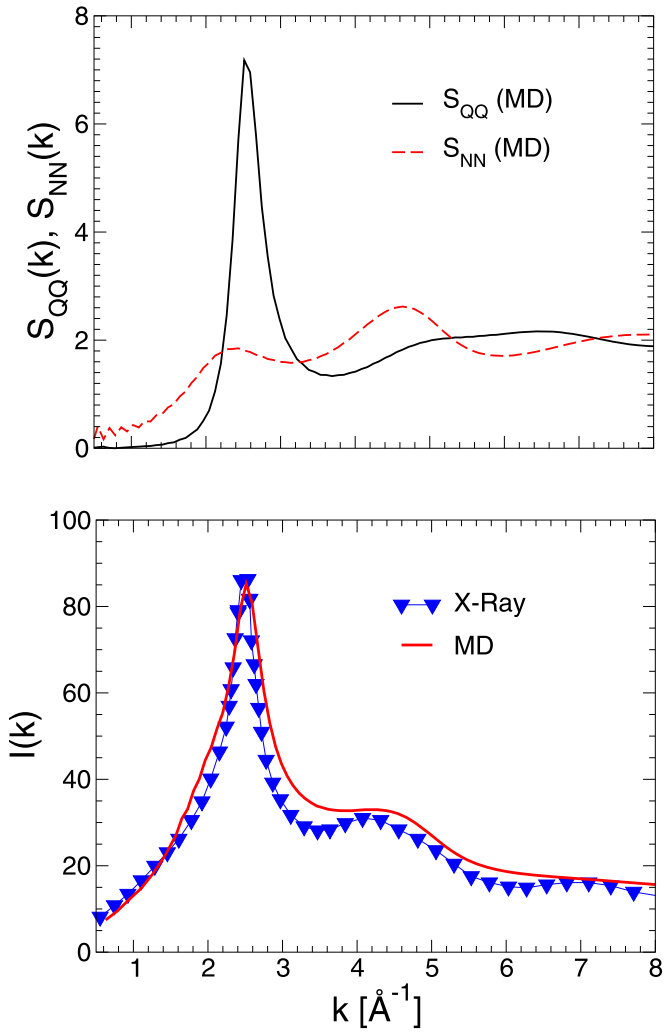

Figure 6. Structural properties of LiF at $T = 1133$ K from MD (lines) and x-rays (triangles down) [31].

The $S_{ij}(k)$ wherefrom $I(k)$ has been determined are then shown in the top panel of figure 7 together with those pertaining to the TF $\alpha = 3.03$. We see that the main features and oscillations of the $\alpha = 5$ structure factors are emphasized and shifted to lower k with respect to the TF ones. The overall enhancement of the $S_{ij}(k)$ is clearly responsible for the just observed overestimate of the $I(k)$ main peak. Nonetheless, the $S_{ij}(k)$ do now favorably combine so to yield a $S_{NN}(k)$ whose first maximum falls at $k \simeq 2.7$ Å^{-1}, in agreement with the wavevector of the maximum in the experimental $I(k)$ (see central and bottom panel of figure 7).

The shift of the $S_{ij}(k)$ features to low k indicates interparticle correlations holding on longer distances than predicted by the standard BHMFT description. This is clearly illustrated by the behavior of the radial distribution functions $g_{ij}(r)$, which we show in figure 8.

It appears that both $g_{\mathrm{NaNa}}(r)$ and $g_{\mathrm{NaF}}(r)$ are characterized by significantly more persistent tail oscillations, while the first unlike coordination shell in $g_{\mathrm{NaF}}(r)$ appears expanded by approximately $\simeq$20%. This also emerges from the inset of the bottom panel of figure 8, where we show the total density-density radial distribution function $g_{\mathrm{NN}}(r)$ defined through equation (9). As is clear, for $\alpha = 5$ the main peak of this function falls at a distance larger than what found in the TF α case, namely at $r = 2.32$ Å. Obviously, this peak is correlated with the first maximum of $S_{\mathrm{NN}}(k)$—considering that 2.7 Å$^{-1} = 2\pi/(2.32$ Å)—and hence to the maximum of the experimental $I(k)$.

We finally illustrate the case of molten KF. The MD $g_{ij}(r)$ we calculate on the basis of the standard BHMFT description, compare quite satisfactorily with previous similar estimates [12]; the latter, however, were already found unable to reproduce correctly some features of the 'experimental' $g_{ij}(r)$ [12]. Those inadequacies now emerge even more markedly, after we compute $I(k)$ from our MD $S_{ij}(k)$. Indeed, similarly to what we have found in NaF, the x-ray diffraction intensity turns out sensibly discrepant with respect to the experimental pattern, as visible in figure 9. Also in this case stiffening the potential at short range gives rise to a qualitative improvement

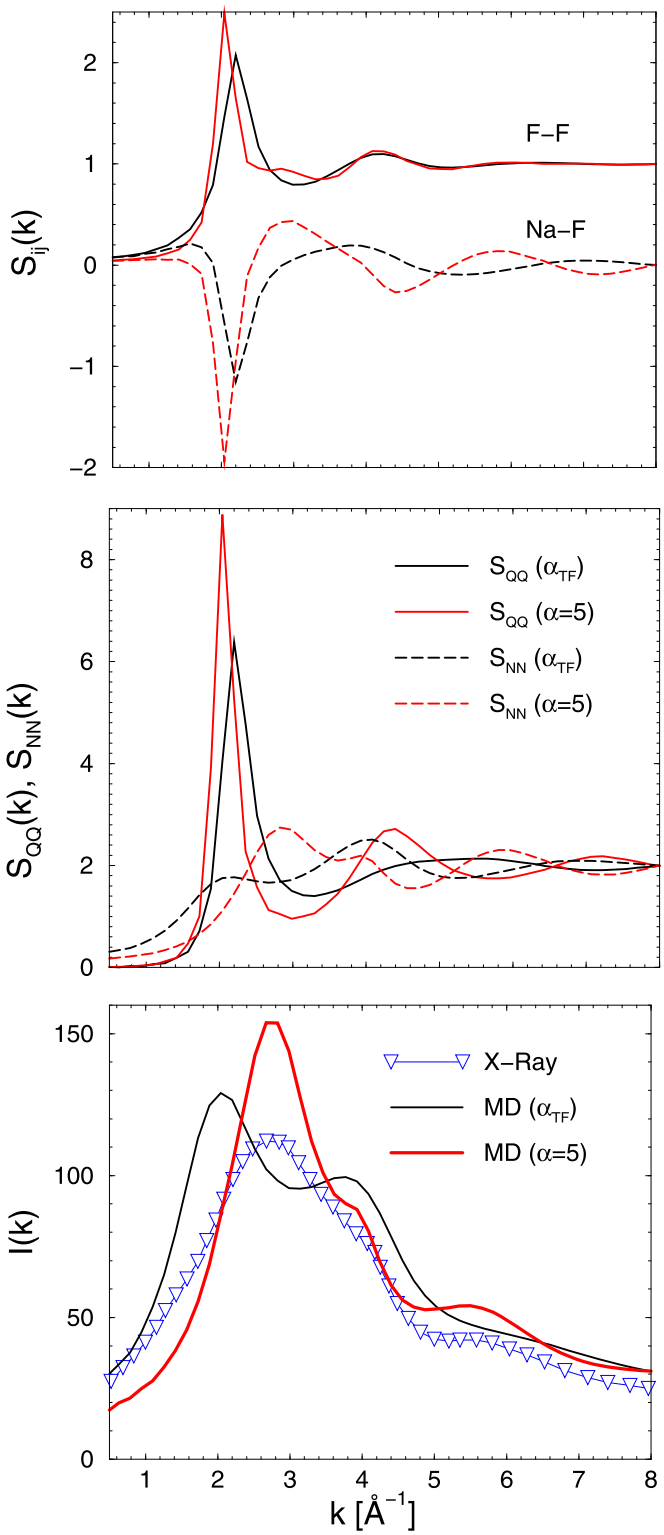

Figure 7. Structural properties of NaF at $T = 1273$ K from MD with $\alpha = \alpha_{TF}$ (black lines), $\alpha = 5$ (red lines) and x-rays (triangles down) [31]. In the top panel, $S_{NaNa}(k)$ practically overlaps with $S_{FF}(k)$ and is not displayed.

of $I(k)$. In particular, we recover the double peak structure of the experimental $I(k)$ although, similarly to NaF, the overall pattern is placed appreciably above the real x-ray diffraction intensity.

It seems possible to infer, from the results for molten NaF and KF, that the BHM form of the potential is still a suitable interaction law for these systems provided a stiffer short range repulsion is adopted, as actually implied by the increase of the α exponent. In this respect, we recall that in the solid configuration of the alkali halides the BHMFT potential works quite satisfactorily [8]. When applied to the molten state that scheme still appears successful for LiF, as shown above. Its inadequacy for molten NaF and KF indicates that, for these two systems,

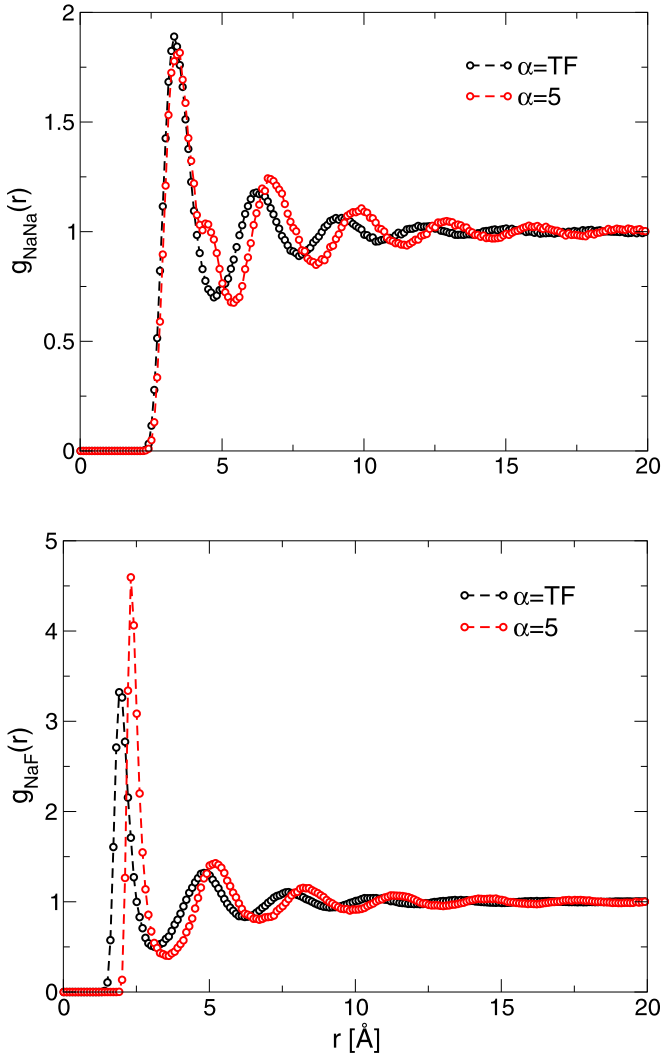

Figure 8. MD radial distribution functions (rdfs) of NaF at $T = 1273$ K obtained with different values of the α exponent. Top; 'like' rdf $g_{\mathrm{NaNa}}(r)$; $g_{\mathrm{FF}}(r)$ is not shown because it overlaps to $g_{\mathrm{NaNa}}(r)$. Bottom: 'unlike' rdf $g_{\mathrm{NaF}}(r)$ Inset: total density-density rdf $g_{\mathrm{NN}}(r)$ (see section 2 and note [39]).

whenever ions of opposite sign are free to move as in a liquid, they tend to come too close so that a correction of the repulsive interaction at short range is required. This is not necessary in LiF, plausibly because of the small size of Li^{+}. As far as the actual value of the α parameter employed in molten NaF and KF is concerned, we have admittedly fixed it via an empirical best fit procedure. A more rigorous determination could probably be attempted, for the present and other fluoride salts, as well as for other molten alkali halides, via a systematic fit of the experimental excess internal energies of these systems. Unfortunately, these are not always available, or are available only close to the melting temperature. Such an investigation will form the subject of a forthcoming study.

We note that in our previous paper [7] we found it necessary to vary other parameters of the BHMFT potential, namely the FT ionic sizes, in order to reproduce at a quantitative level the liquid-vapor phase diagram of NaCl and KCl, and the isothermal compressibilities of a number of molten salts. We have verified that the BHMFT potential, with such modified FT ionic radii, leads to $S_{ij}(k)$ that are practically identical to those obtained with the standard FT ionic sizes. Moreover, there is no appreciable effect on the MD $I(k)$, overlapping in the two parametrizations.

It is worth to summarize the results hitherto illustrated so as to highlight common features across the six molten salts examined. We first focus on the relatively low wavevector region ($k \leqslant 3$ Å^{-1}) of $I(k)$ of NaCl, RbCl and KF. As is visible in figures 3, 4 and 9, all these salts show for 1.4 Å$^{-1} \leqslant k \leqslant 2.4$ Å^{-1} a 'double peak structure' and, as we have seen, for NaCl and RbCl the first of these two peaks falls at the same k of the main (aligned) features of the neutron $a_{ij}(k)$. Our MD analysis is able to correctly reproduce such experimental outcomes and highlights that the first peak in $I(k)$ actually also falls in correspondence with the main peak in both the neutron and MD $S_{\mathrm{QQ}}(k)$ of NaCl and RbCl. As for KF, for which no neutron $a_{\mathrm{ij}}(k)$ exist to compare with, we show on the

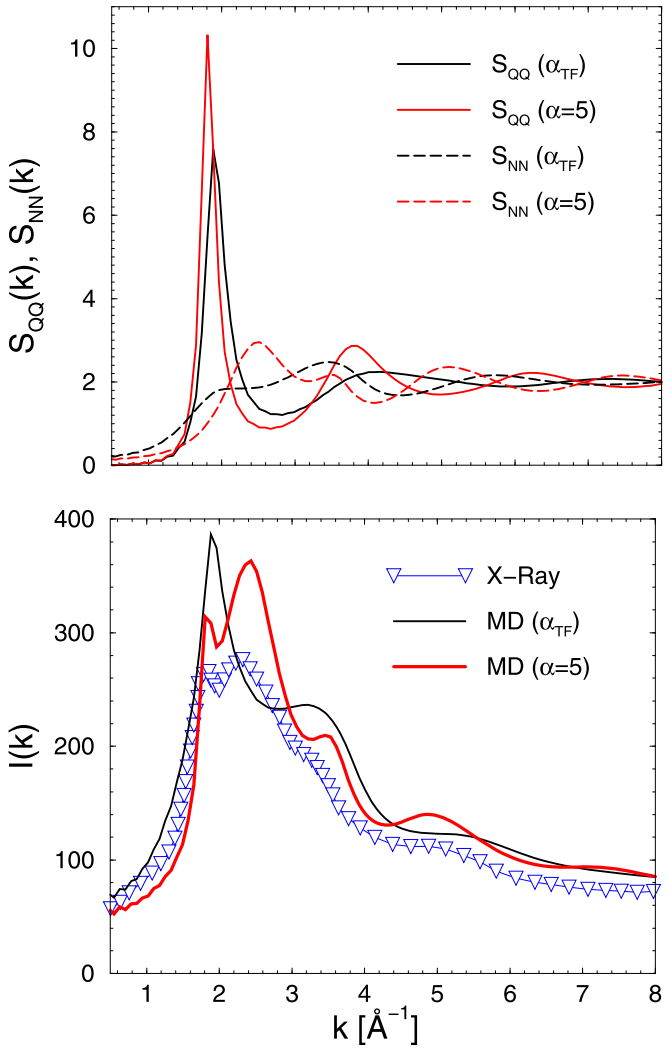

Figure 9. Structural properties of KF at $T = 1143$ K from MD with $\alpha = \alpha_{TF}$ (black lines), $\alpha = 5$ (red lines) and x-rays (triangles down) [31].

basis of our MD evidence that the coincidence of peak positions equally holds. For the same three salts, the second of the twin peaks falls in correspondence with the first maximum of the neutron determined $S_{NN}(k)$. Again. the MD calculations reproduce quite well the experimental $S_{NN}(k)$.

Moving to the $I(k)$ of molten LiCl and LiF (see figures 5 and 6), these experimental patterns appear characterized by a sharp peak falling in the range $2\ \text{Å}^{-1} \leqslant k \leqslant 2.5\ \text{Å}^{-1}$. It emerges from the neutron data for LiCl, that the position of this peak coincides with the main features of the $a_{ij}(k)$, and hence with the main peak of $S_{QQ}(k)$, as it happened in NaCl and RbCl. The MD calculations reproduce quite well this outcome for LiCl, and signal that a similar coincidence takes place in LiF, whose $I(k)$ is quite well predicted. Moreover, our investigation documents that the considerable height of the first peak in $I(k)$ is the consequence of the coincidence of the first maxima in $S_{NN}(k)$ and $S_{QQ}(k)$.

Finally, in NaF (see figure 7) $I(k)$ exhibits a broad maximum for $k \simeq 2.7\ \text{Å}^{-1}$. At variance with all the previous cases, we here find that this feature does not fall in correspondence of the first peaks in $S_{QQ}(k)$ and $S_{ij}(k)$, but rather falls in coincidence of the first maximum in the MD $S_{NN}(k)$; indeed, for this salt characterized by iso-electronic ions Na^+ and F^-, the contribution to the scattered x-ray intensity associated to $S_{QQ}(k)$ (amounting to $C_{QQ}(k)$), practically vanishes because of the strong similarity of the atomic form factors.

Moving to the high k region, all the experimental $I(k)$ of the six salts we have examined exhibit a broad second (third) maximum or a shoulder, in the range $3.5\ \text{Å}^{-1} \leqslant k \leqslant 5.5\ \text{Å}^{-1}$. We have shown that this feature invariably correlates in position to the second maximum of both the experimental and MD $S_{NN}(k)$.

It is useful to observe that two different model potentials can both reproduce the experimental k-space patterns with small *different* discrepancies. For the same reason, their comparison with the neutron or x-ray diffraction patterns might not be sufficient to decide whether one model is superior to the other. The situation would be different, however, if one model provides predictions in marked contrast with the k-space

experimental data. In this case r-space predictions [e.g. $g_{ij}(r)$], even if apparently reliable, should be looked at with some caution. Actually, it seems reasonable to suggest that the comparison here made with neutron partial structure factors and with x-ray intensities—which last, as noted, can be obtained from equation (10)—is worth to be undertaken for *any* model potential of molten alkali halides. We have tried to show that such calculations are nowadays accurately feasible in the context of a simulation approach.

As for the MD algorithm employed for the present simulation investigation, we consider the structural analysis hereby performed as a preliminary step towards the calculation, which we plan for a forthcoming paper, of dynamical and transport properties, like ionic self-diffusion and viscosity coefficients, which are quantities of specific technological interest for, e.g., the efficiency of last generation nuclear reactors [1–3].

4. Conclusions

Through extensive MD simulations we have performed an investigation of the accuracy of the BHMFT model in describing the wavevector dependent properties of six molten alkali halides. In three of these systems, namely NaCl, RbCl and LiCl, the MD partial structure factors have been assessed against their experimental counterparts as obtained by neutron diffraction. For the same salts the x-ray diffraction intensity $I(k)$ has then been derived from the MD $S_{ij}(k)$, and compared to experimental data. We have found that in any case the BHMFT model is able to yield rather accurate predictions.

Investigation has then been extended to molten fluorides, namely LiF, NaF and KF. Here no neutron diffraction data are available and the comparison with experimental data has been possibile only for the x-ray diffraction intensity. For LiF the agreement of the MD $I(k)$ with experiment is satisfactory. For NaF and KF the BHMFT potential with the crystal FT parameters doesn't predict correctly the experimental patterns; however, when the potential is stiffened at short range through a variation of the exponential repulsive parameter, we recover qualitative agreement between the MD $I(k)$ and the experimental one. An intervention on other FT parameters entering the BHMFT potential, namely the ionic sizes, has also been recently performed by us in [7]; we have thereby been able to obtain the liquid-vapor phase diagram of NaCl and KCl in quantitative agreement with experiment. Therefore, it seems possible to obtain a qualitatively accurate description of different properties of molten alkali halides by modifying different FT parameters in the BHMFT interaction law.

By then reconsidering the correlations outlined at the end of the previous section between the $I(k)$ and the structure factors' features, we argue that these might also hold for other salts of the alkali halide family. This seems possible because of the similarities emerging in the experimental $I(k)$ patterns: specifically, the double peak structure found in molten NaCl, RbCl and KF, is also present in the $I(k)$ of CsCl [34], KI and RbI [33], while the unique sharp peak at relatively small k visible in LiCl and LiF, is also seen in LiI, LiBr, and NaI [34]; finally, salts formed by two iso-electronic ions as KCl, RbBr and CsI have $I(k)$ that are similar to that of NaF. We surmise that a wide investigation of all these molten alkali halides might produce valuable structural information, which could worthly complement the ample interpretative work, developed along several decades, of x-ray diffraction experimental data.

We finally observe that limitations of the BHMFT scheme were already highlighted in the past when polarizable ion models were proposed [14]. It is also worth noting that more sophisticated approaches to molten alkali halides description, and in particular of molten fluorides, have been recently devised in terms of *ab-initio* potentials [44–48]. Nonetheless, given the relative simplicity of the model description here adopted, and the interpretative hints that can be provided for the experimental evidences, we plan further applications of the simulation approach here proposed. Future investigations along this direction could provide an assessment of a number of structural predictions, amply produced in the past at the level of radial distribution functions of systems for which no neutron diffraction studies are available, and no direct comparison with the x-ray experimental evidence has been performed.

Acknowledgments

This work has been done using the computer facilities made available by the PO-FESR 2007-2013 Project MedNETNA (Mediterranean Network for Emerging Nanomaterials).

ORCID iDs

Dino Costa https://orcid.org/0000-0001-8647-9574
Gianmarco Munaò https://orcid.org/0000-0002-7206-3233
Santi Prestipino https://orcid.org/0000-0002-6266-7025
Carlo Caccamo https://orcid.org/0000-0001-8460-6410

References

[1] Mathieu L *et al* 2006 *Prog. Nucl. Energy* **48** 664
[2] Serp J *et al* 2014 *Prog. Nucl. Energy* **77** 308
[3] Heuer D, Merle-Lucotte E, Alibert M, Brovchenko M, Ghetta V and Rubiolo P 2014 *Ann. Nucl. Energy* **64** 421
[4] Song J, Shi S, Li X and Yan L 2017 *J. Mol. Liq.* **234** 279
[5] Nunes V M B, Queiros C S, Lourenco M J V, Santos F J V and Nieto de Castro C A 2016 *Appl. Energy* **183** 603
[6] Myers P D and Goswami D Y 2016 *Appl. Therm. Eng.* **109** 889
[7] Abramo M C, Costa D, Malescio G, Munaò G, Pellicane G, Prestipino S and Caccamo C 2018 *Phys. Rev.* E **98** 010103
[8] Tosi M P and Fumi F 1964 *J. Phys. Chem. Solids* **25** 31
[9] Woodcock L V and Singer K 1971 *Trans. Faraday Soc.* **67** 12
[10] Lewis J W E, Singer K and Woodcock L V 1975 *J. Chem. Soc. Faraday Trans. II* **71** 301
[11] Lewis J W E and Singer K 1975 *J. Chem. Soc. Faraday II* **71** 41
[12] Adams D J and McDonald I R 1974 *J. Phys. C: Solid State Phys* **7** 2761
[13] Adams D J 1976 *J. Chem. Soc., Faraday Trans. II* **72** 1372
[14] Sangster M J L and Dixon M 1976 *Adv. Phys.* **25** 247
[15] Copley J R D and Rahman A 1976 *Phys. Rev.* A **13** 2276
[16] Dixon M and Gillan M J 1981 *Phil. Mag.* B **43** 1099
[17] Caccamo C and Dixon M 1980 *J. Phys. C: Solid State Phys.* **13** 1887
[18] Luo H, Xiao S, Wang S, Haio P, Deng H and Hu W 2016 *Comput. Mat. Sci.* **111** 203
[19] Wang J, Wu J, Lu G and Yu J 2017 *J. Mol. Liq.* **238** 236
[20] Su Z, Cai L, Ni H, Lu G, Song X and Wu J 2018 *J. Appl. Electroch.* **48** 1175
[21] Wu J, Wang J, Ni H, Lu G and Yu S 2018 *J. Mol. Liq.* **253** 96
[22] Baranyai A, Ruff I and McGreevy R L 1986 *J. Phys. C: Solid State Phys.* **19** 453
[23] Edwards F G, Enderby J E, Rowe R A and Page D I 1975 *J. Phys. C: Solid State Phys* **8** 3483
[24] Derrien J I and Dupuy J 1975 *J. Phys. (Paris)* **36** 191
[25] Mitchell E W, Poncet P F J and Stewart R J 1976 *Phil Mag.* **34** 721
[26] Locke J, Messoloras S, Stuart R J, McGreevy R L and Mitchell E W J 1985 *Phil. Mag.* B **51** 301
[27] Howe M A and McGreevy R L 1988 *Phil. Mag.* B **58** 485
[28] McGreevy R L and Howe M A 1989 *J. Phys.: Condens. Matter* **1** 9957
[29] Saito M, Kang S and Waseda Y 1999 *Jpn. J. Appl. Phys.* **38** 596
[30] Tahara S, Ohara K, Shimakura H and Fukami T 2017 *EPJ Web of Conferences* **151** 03006
[31] Zarzycki J 1957 *J. Phys. Phys. Appl.* **18** 65
[32] Zarzycki J 1958 *J. Phys. Phys. Appl.* **19** 13
[33] Antonov B D 1975 *J. Struct. Chem.* **16** 474
[34] Levy H A, Agron P A, Bredig M A and Danford M D 1960 *Ann. New York Acad. Sci.* **79** 762
[35] Abramo M C, Caccamo C, Pizzimenti G, Parrinello M and Tosi M P 1978 *J. Chem. Phys.* **68** 2889
[36] Allen M P and Tildsley D J 1987 *Computer Simulation of Liquids* (Oxford: Clarendon)
[37] March N H and Tosi M P 1976 *Atomic Dynamics in Liquids* (London-Basingstoke: MacMillan Press LTD)
[38] Bhatia A B and Thornton D E 1970 *Phys. Rev.* B **2** 2004
[39] The standard expressions of $S_{\rm QQ}(k)$, $S_{\rm NN}(k)$ and $g_{\rm NN}(r)$ (see ref. 37 and 38) differ from those here adopted for a multiplying factor $\frac{1}{2}$. We are thus employing a magnification that turns out useful in the grafical representations following below. The true asymptotic limit, $k \to \infty / r \to \infty$, of the above functions is obviously 1.
[40] Price D L and Copley J R D 1975 *Phys. Rev.* A **11** 2124
[41] International tables of x-ray Crystallography vol. III (International Union of Crystallography, The Kynoch Press, Birmingham, 1967).
[42] Compton A H and Allison S K 1960 *X-rays in Theory and Experiment* (Princeton: Van Nostrand)
[43] Ballone P, Pastore G and Tosi M P 1984 *J. Chem. Phys.* **81** 3174
[44] Wilson M and Madden P A 1993 *J. Phys.: Condens. Matter* **5** 2687
[45] Madden P A, Heaton R, Aguado A and Jahn S 2006 *J. Mol. Structure: TEOCHEM* **771** 9
[46] Salanne M, Simon C, Turq P and Madden P A 2009 *J. Fluor. Chem.* **130** 38
[47] Dewan L C, Simon C, Madden P A, Hobbs L W and Salanne M 2013 *J. Nucl. Mat.* **434** 322
[48] Mukhopadhyay S and Demmel F 2018 *AIP Conf. Proc.* **1969** 030001